Journal of Chromatography A, 1217 (2010) 6578–6587

Contents lists available at ScienceDirect

Journal of Chromatography A

journal homepage: www.elsevier.com/locate/chroma

Numerical modeling of elution peak profiles in supercritical fluid chromatography. Part I—Elution of an unretained tracer

Krzysztof Kaczmarski[a,*], Donald P. Poe[b], Georges Guiochon[c,d]

[a] Department of Chemical and Process Engineering, Rzeszów University of Technology, 35-959 Rzeszów, Poland
[b] Department of Chemistry and Biochemistry, University of Minnesota Duluth, Duluth, MN 55812, USA
[c] Department of Chemistry, University of Tennessee, Knoxville, TN 37996-1600, USA
[d] Division of Chemical Sciences, Oak Ridge National Laboratory, Oak Ridge, TN, USA

ARTICLE INFO

Article history:
Received 19 June 2010
Received in revised form 11 August 2010
Accepted 12 August 2010
Available online 19 August 2010

Keywords:
Supercritical fluid chromatography
Axial temperature profiles
Column efficiency
Expansion cooling
Heat balance
Heat generation
Heat transfer
Peak profiles
Radial temperature profiles
Viscous friction

ABSTRACT

When chromatography is carried out with high-density carbon dioxide as the main component of the mobile phase (a method generally known as "supercritical fluid chromatography" or SFC), the required pressure gradient along the column is moderate. However, this mobile phase is highly compressible and, under certain experimental conditions, its density may decrease significantly along the column. Such an expansion absorbs heat, cooling the column, which absorbs heat from the outside. The resulting heat transfer causes the formation of axial and radial gradients of temperature that may become large under certain conditions. Due to these gradients, the mobile phase velocity and most physico-chemical parameters of the system (viscosity, diffusion coefficients, etc.) are no longer constant throughout the column, resulting in a loss of column efficiency, even at low flow rates. At high flow rates and in serious cases, systematic variations of the retention factors and the separation factors with increasing flow rates and important deformations of the elution profiles of all sample components may occur. The model previously used to account satisfactorily for the effects of the viscous friction heating of the mobile phase in HPLC is adapted here to account for the expansion cooling of the mobile phase in SFC and is applied to the modeling of the elution peak profiles of an unretained compound in SFC. The numerical solution of the combined heat and mass balance equations provides temperature and pressure profiles inside the column, and values of the retention time and efficiency for elution of this unretained compound that are in excellent agreement with independent experimental data.

1. Introduction

Supercritical fluid chromatography (SFC) is currently undergoing a period of renewed interest because it is considered as a "green" alternative to classical preparative liquid chromatography, due to its use of a mobile phase based on high-density CO_2. Although organic solvents must often be added to the CO_2 as modifiers (which means that most mobile phases are actually not supercritical), their required concentrations are lower than in HPLC. Other advantages of SFC are the ease with which the solvent properties can be adjusted by changing the operating pressure and temperature, the low viscosity of the mobile phase, and the high diffusivity of the sample components that result in mass transfer resistances that are lower than in similar systems used in classical HPLC. For these reasons, SFC often permits the achievement of faster and more efficient separations than HPLC and provides higher production rates in preparative applications. SFC has become widely used for the separation of enantiomers for the production of pharmaceutical intermediates [1]. Applications of SFC, however, are neither restricted to this type of compounds nor to periodic separations and there seems to be much future in SFC-based simulated moving bed processes [2,3].

To improve the speed of analyses and the separation power of columns in all the forms of chromatography, gas chromatography, SFC, and HPLC, analysts have always tried to use smaller and smaller particles. This evolution has moved by leaps and bounds in the past. A major acceleration of this trend took place a few years ago, with the development of a generation of sub-2 μm particles and a series of new superficially porous or shell particles. Besides considerably improved column performance, this trend brings to analysts new, serious, sometimes unexpected difficulties. One universal difficulty, which will not be discussed here, is related to the decrease in the volume and time-widths of analyte peaks, which are eluted faster from shorter columns, a decrease that is due to the use of the new very fast, short, efficient columns. This decrease requires

* Corresponding author. Tel.: +4817 8651295; fax: +4817 854 36 55.
E-mail addresses: kkaczmarski@prz.edu.pl, kkaczmarski@prz.rzeszow.pl (K. Kaczmarski).

0021-9673/$ – see front matter © 2010 Elsevier B.V. All rights reserved.
doi:10.1016/j.chroma.2010.08.035

important reductions in the extra-column volumes of instruments and in their response times to prevent their contributions from spoiling the gains in resolution.

Other serious difficulties arise from the increase of the mobile phase velocity at which these new columns must be operated, because the optimum mobile phase velocity of a column increases with decreasing particle size, which is why finer particles are needed. However, the column permeability decreases with decreasing square of the particle diameter, so modern HPLC columns must be run at high inlet pressures, meaning under a high pressure gradient. The combination of a high pressure gradient and a high eluent velocity results in the production of an intense amount of heat. This heat tends to leave the column, causing the formation of axial and radial temperature gradients. So, potentially intense axial and radial gradients of all physico-chemical parameters appear.

We previously developed and validated a model combining the heat and the mass balance equations of HPLC columns, an isotherm model for the analyte, and the equations accounting for flow in porous media [4,5]. This model accurately predicts analyte retention factors, their elution band profiles, and the dependence of the column efficiency on the mobile phase velocity. Similar improvements in the efficiency and speed of SFC separations require the operation of the columns used at high mobile phase velocities. This means that, in spite of the low viscosity of the SFC mobile phase, significant pressure gradients take place along the column. However, when large pressure drops are applied in packed-column SFC, excessive efficiency losses may occur, as reported by several authors [6–12], while others have reported no significant loss in performance [13–17]. Good agreement was generally obtained when comparing experimental results and the predictions of semi-empirical models but only as long as the outlet pressure exceeded about 130 bar [6–9]. At lower outlet pressures, poorly shaped peaks and poor agreement with theory were observed. The loss of efficiency observed under these conditions places important practical limits on operating conditions for packed-column SFC. This is unfortunate because at lower pressures, increased diffusivity and decreased viscosity and density favor increased speed and efficiency. Excess efficiency loss in SFC has recently been attributed to effects of radial density and temperature changes on the retention factor [18,19].

The goal of this work is to adapt the model developed for very high pressure liquid chromatography (VHPLC) to SFC conditions and to investigate the validity of this new heat and mass transfer model under the typical experimental setting used in SFC. For this purpose, we first compared the temperature recorded at the external surface of outlet column endfitting and pressure drop inside column with those calculated with our model. Afterwards we compared the measured and simulated retention time of unretained solute and column efficiency in a wide interval of mobile phase flow. Good agreement between experimental results and theory was obtained. We report also on the distributions of axial and radial temperature, density, viscosity and fluid velocity distribution.

2. Mathematical models

The modeling problems encountered in SFC are very similar to those previously solved in the case of VHPLC. However, the influences of the pressure and the temperature on the physico-chemical parameters of a chromatographic system are more important in SFC than in VHPLC. In this work, we adopted the VHPLC model developed in our previous papers [4,5]. Similarly to the VHPLC model, this SFC model combines three separate models: (1) a model of heat transfer; (2) a model of mass transfer; and (3) a model of mobile phase velocity distribution. These three models must be solved together. The first model expresses how heat is absorbed during the expansion of the mobile phase, how it is simultaneously generated by viscous friction, and how it is transferred into or out of the column under steady-state conditions. The second model accounts for the propagation of a compound band along a column in which there are gradients of temperature, viscosity, velocity, density and other parameters. This model includes an isotherm model, the equilibrium constants of which depend on the local temperature and the mobile phase density. The third model accounts for the distribution of the mobile phase velocity, which depends on the local temperature, pressure, viscosity and density and is given by the equations of hydrodynamics in porous media.

Due to the considerable changes in the physico-chemical parameters that take place in SFC and were already discussed elsewhere for HPLC [4,5], the heat and the mass transfer models had to be modified, as explained in the next sections. On the other hand, the model for the distribution of the mobile phase velocity is exactly the same as the one presented in [4], so it will be discussed here only briefly.

2.1. The heat balance equation

In formulating the heat balance equation, we assume that heat is generated inside the column, due to the viscous friction of the mobile phase percolating through the bed, and that it is, at the same time, absorbed by the expansion of the mobile phase. Moreover, heat is conducted from the column surroundings, through the column wall, into the packed bed and the mobile phase. The model assumptions are the following:

1. for packed beds, axial heat dispersion and axial heat conductivity are negligible,
2. local, radial heat transfer is expressed by the local, effective radial conductivity,
3. the mobile phase flow velocity is a function of both the radial and the axial coordinates but the mobile phase mass flux is constant in the axial direction,
4. pressure is a function of the axial direction but is constant in the radial direction,
5. heat is conducted in both the axial and the radial directions of the column tube.

2.1.1. Equations

Under this set of assumptions, the heat balance for an infinitesimal volume element of a packed bed is written in a system of cylindrical coordinates as [4,5,20–23]:

$$(\varepsilon_t c_p^m + (1-\varepsilon_t)c_s)\frac{\partial T}{\partial t} - \varepsilon_t T\alpha\frac{\partial P}{\partial t} + c_p^m u_z\frac{\partial T}{\partial z} + c_p^m u_r\frac{\partial T}{\partial r} = \frac{1}{r}\frac{\partial}{\partial r}\left(r\lambda_{r,ef}\frac{\partial T}{\partial r}\right) - u_z(1-\alpha T)\frac{\partial P}{\partial z} \quad (1)$$

where ε_t is the total column porosity, c_p^m is the mobile phase heat capacity (J/m^3/K), c_s is the solid phase heat capacity (J/m^3/K), T is the local temperature (K), P is the pressure (bar), u_z is the superficial velocity of the mobile phase in the axial direction (m/s), u_r is the superficial velocity of the mobile phase in the radial direction (m/s)—the radial velocity comes from radial temperature gradient, and $\lambda_{r,ef}$ is the effective bed conductivity (W/m/K). The coefficient α (K^{-1}) is the coefficient of thermal expansion of the mobile phase. It is important to remember that all these parameters are functions of the position in the column and the time.

The heat generated inside the column due to viscous friction is the product of the superficial velocity and the pressure gradient:

$$h_g = -u_z \frac{\partial P}{\partial z} \tag{2a}$$

The heat consumed by the expansion of the fluid is equal to:

$$h_c = u_z \alpha T \frac{\partial P}{\partial z} \tag{2b}$$

The coefficient of thermal expansion is calculated from the equation:

$$\alpha = -\frac{1}{\rho}\frac{\delta \rho}{\delta T} \tag{2c}$$

The heat balance for the column wall can be formulated as follows:

$$c_w \frac{\partial T}{\partial t} = \lambda_w \left[\frac{1}{r}\frac{\partial T}{\partial r} + \frac{\partial^2 T}{\partial r^2}\right] + \lambda_w \frac{\partial^2 T}{\partial z^2} \tag{3}$$

where c_w is the wall heat capacity (J/m^3/K), and λ_w is the wall heat conductivity (W/m/K).

2.1.2. Initial and boundary conditions

The initial and the boundary conditions of the system of Eqs. (1) and (3) are formulated as follows:

- Initial condition

$$\text{for} \quad t = 0, \quad \text{we have:} \quad T(r,z) = T_{ext} \tag{4}$$

- *Boundary conditions for Eq. (1)* for $t > 0$, we have:

$$\text{at} \quad z = 0, \quad T(r,z) = T_0 \tag{5a}$$

$$\text{at} \quad z = L, \quad \frac{\partial T}{\partial z} = 0 \tag{5b}$$

$$\text{at} \quad r = 0, \quad \frac{\partial T}{\partial r} = 0 \tag{5c}$$

$$\text{at} \quad r = R_i, \quad \lambda_{r,ef}\frac{\partial T}{\partial r} = \lambda_w \frac{\partial T}{\partial r} \tag{5d}$$

where T_{ext} is the air thermostat temperature, T_0 is the mobile phase temperature at the column inlet, L is the column length (m), and R_i is the internal column wall radius (m).

- *Boundary conditions for Eq. (3)* for $t > 0$,

$$\text{at} \quad z = 0, \quad \lambda_w \frac{\partial T(r,z)}{\partial z} = 0 h_c (T_{ext} - T_w(r,z)) \tag{6a}$$

$$\text{at} \quad z = L, \quad \lambda_w \frac{\partial T(r,z)}{\partial z} = h_e (T_{ext} - T_w(r,z)) \tag{6b}$$

$$\text{at} \quad r = R_i, \quad \lambda_{r,ef}\frac{\partial T(r,z)}{\partial r} = \lambda_w \frac{\partial T(r,z)}{\partial r} \tag{6c}$$

$$\text{at} \quad r = R_e, \quad \lambda_w \frac{\partial T(r,z)}{\partial r} = h_e (T_{ext} - T(r,z)) \tag{6d}$$

where R_e is the external column wall radius (m) and h_e is the effective heat transfer coefficient (W/m^2/K) between the external surface of the column tube and the air outside column. In the case of an insulated column, the coefficient h_e was taken as equal to zero.

Under steady-state conditions, the heat balance model can be simplified by neglecting the time dependent terms (the first two terms in Eq. (1) and the first term in Eq. (3)) and the initial conditions.

2.2. The mass balance equation

In writing the mass balance for an analyte, we assume that the contributions to band broadening due to the finite mass transfer resistances and to apparent axial dispersion can be lumped into an apparent dispersion coefficient. This coefficient must be evaluated using formulae developed in [5,24]. It should be also remembered that axial dispersion, radial dispersion and velocity are functions of the position inside the column. Under this assumption, the mass balance equation is an extension of the Equilibrium-Dispersive (ED) model [25].

The mass balance equation of the generalized ED model is written as follows:

$$\frac{\partial C}{\partial t} + F\frac{\partial q}{\partial t} + \frac{\partial (w_z C)}{\partial z} = \frac{\partial}{\partial z}\left(D_{z,a}\frac{\partial C}{\partial x}\right) + \frac{1}{r}\frac{\partial}{\partial r}\left(r D_{r,a}\frac{\partial C}{\partial r}\right) \tag{7}$$

where C and q are the analyte concentrations in the mobile and in the stationary phases at equilibrium (g/L), respectively, $D_{z,a}$ and $D_{r,a}$ are the local axial and radial apparent dispersion coefficients (m^2/s), respectively, $w_z = u_z/\varepsilon_t$ (m/s) is the interstitial velocity, $F = (1-\varepsilon_t)/\varepsilon_t$ is the phase ratio and ε_t is the total porosity of the column. In the model of mass transfer, the radial velocity was neglected because is about 0.001 of the value of the axial velocity (see Section 4).

In earlier papers [5], it was proved that the solution of the generalized ED model is compatible with the general rate or the pore diffusion model when the axial apparent dispersion coefficient is calculated from the following equation:

$$D_{z,a} = \frac{D_L \varepsilon_e}{\varepsilon_t} + \left(\frac{k_1}{1+k_1}\right)^2 \frac{u^2 d_p}{\varepsilon_t \varepsilon_e F_e 6}\left[\frac{d_p}{10 D_{eff}} + \frac{1}{k_{ext}}\right] \tag{8}$$

where

$$k_1 = F_e\left(\varepsilon_p + (1-\varepsilon_p)\frac{\delta q}{\delta C}\right); \qquad F_e = \frac{1-\varepsilon_e}{\varepsilon_e}; \qquad D_{eff} = \frac{D_m \varepsilon_p}{\tau} \tag{9}$$

and D_L is the axial dispersion coefficient, D_m is the molecular diffusion coefficient, ε_e is the external porosity, ε_p is the particle porosity, τ is the tortuosity coefficient and k_{ext} is the external mass transfer coefficient (see Section 2.4.2).

The apparent radial dispersion coefficient, $D_{a,r}$, was calculated on the basis of the plate height equation derived by Knox [26,27].

$$D_{r,a} = \frac{0.03 d_p u}{\varepsilon_t} + 0.7 D_m \tag{10}$$

where D_m is the molecular diffusion coefficient and d_p is the adsorbent particle diameter.

It should be noted that all the dispersion and diffusion coefficients are functions of the position inside the column.

The model (7) was solved with the typical initial and boundary conditions:

- Initial conditions, for $t = 0$

$$C(0,r,z) = q(0,r,z) = 0 \tag{11}$$

- Boundary conditions.for $t > 0$; $z = 0$

$$C(0) = \begin{cases} C_F & \text{for} \quad 0 < t < t_p \\ 0 & \text{for} \quad t > t_p \end{cases} \tag{12}$$

for $t > 0$; $z = L$

$$\frac{\partial C}{\partial z} = 0 \tag{13}$$

for $t > 0$, $r = R_p$ and $r = 0$

$$\frac{\partial C}{\partial r} = 0 \tag{14}$$

where t_p is the injection time (s), R_p the particle radius (m), and the subscript F denotes the inlet value.

Eq. (7) must be combined with an appropriate isotherm equation. In this work, we consider only the retention of an inert species, so it was assumed that $q = 0$.

2.3. Mobile phase velocity distribution and pressure calculation

The local value of the mobile phase velocity was calculated from Eq. [9]:

$$u_z(r,z) = \frac{u^\circ \rho^\circ}{\eta(r,z)(\overline{\rho/\eta})_z} \tag{15}$$

where $(\overline{\rho/\eta})_z$ denotes the average value of the ratio ρ/η at a given axial position,

$$\left(\frac{\bar{\rho}}{\eta}\right)_z = \frac{2}{R_i^2}\int_0^R \frac{\rho(r,z)}{\eta(r,z)}\mathrm{d}r \tag{16}$$

and u°, ρ° are the mobile phase superficial velocity and density at the column inlet.

The local pressure gradient was calculated according to the correlation developed by Blake, Kozeny, and Carman [28], using the following equation [4].

$$-\frac{\delta P}{\delta z} = \xi\frac{(1-\varepsilon_e)^2 u^\circ p^\circ}{\varepsilon_e^3 d_p^2(\overline{\rho/\eta})_z} \tag{17}$$

where ξ is an empirical parameter generally considered as equal to 150 [28].

The above system of equations has to be closed by the following relationship:

$$\Delta P = \int_0^L \left(-\frac{\delta P}{\delta z}\right)\mathrm{d}p \tag{18}$$

where ΔP is the actual pressure drop along the column, measured from the instrument gauges.

The radial mobile phase velocity was computed numerically from the continuity equation [4]:

$$\frac{1}{r}\frac{\partial}{\partial r}(\rho r u_r) + \frac{\partial(\rho u_z)}{\partial r} = 0 \tag{19}$$

2.4. Methods of calculation of the physico-chemical parameters

2.4.1. Heat transfer

Success in the calculation of the temperature, mobile phase velocity, and pressure distributions along the column will be judged by the degree of agreement between these calculated distributions and experimental results. Obviously, this success will strongly depend on the accuracy of the equations used to calculate the density ρ, the viscosity η, the mobile phase heat capacity c_p^m, and the effective bed conductivity $\lambda_{r,ef}$.

In this work, the mobile phase was carbon dioxide. Its density at a given pressure and temperature was calculated with the method described by Span and Wagner [29]. The viscosity was obtained from the correlation given by Fenghour et al. [30]. The thermal conductivity was estimated from the model depicted by Vesovic et al. [31]. Finally the heat capacity was obtained from the correlation presented in [29].

In the case of a two-component heterogeneous system that has a chaotic structure, Zarichnyak and Novikov [32] proposed the following equation for the calculation of the effective conductivity:

$$\lambda_{R,ef} = \varepsilon_t^2\lambda_{elu} + \sigma_x^2\lambda_S + 4\varepsilon_t\varepsilon_S\frac{\lambda_{elu}\lambda_S}{\lambda_{elu}+\lambda_S} \tag{20}$$

In this equation, the porosity ε_s is the ratio of the volume of the solid phase (silica and C8 ligands) in the bed to the geometrical volume of the column, λ_S is the solid phase conductivity and λ_{elu} is the conductivity of the eluent. The same equation was used to calculate the solid phase conductivity λ_S on the basis of the partial volume and the conductivity of silica and the C8 ligands.

2.4.2. Mass transfer

To solve the mass balance equation discussed above, the local values of the external mass transfer coefficient, k_{ext}, the dispersion coefficient D_L, the axial, $D_{a,z}$, and the radial, $D_{a,r}$, apparent dispersion coefficients, and the molecular diffusivity, D_m, must be calculated or estimated.

In this work we calculated k_{ext} from the Wilson and Geankoplis [33] correlation which gives:

$$Sh = \frac{1.09}{\varepsilon_e}Re^{0.33}Sc^{0.33} \tag{21}$$

where $Sh = \frac{k_{ext}d_p}{D_m}$ $\quad Re = \frac{ud_p\rho}{\eta}$ $\quad Sc = \frac{\eta}{\rho D_m}$.

The dispersion coefficient was approximated by the relationship [25]:

$$D_L = \gamma_1 D_m + \gamma_2 u d_p \tag{22}$$

where γ_1 and γ_2 are geometrical constants. It was assumed that $\gamma_1 = 0.7$ [25] whereas γ_2 was estimated from the experimental data.

The molecular diffusion coefficient D_m was estimated from the Wilke-Chang equation with modified constants [34].

$$D_m = 8.6\times10^{-15}\frac{TM_S^{0.5}}{\eta_B V_A^{0.6}} \tag{23}$$

where T is the temperature in Kelvins, M_S is the molar mass of the solvent [g/mol], η is its viscosity in Pa s, V_A is the molar volume the solute at its boiling point [cm^3/mol], and D_m has units of m^2/s.

It should be noticed that all the above parameters are functions of the position inside the column.

The tortuosity parameter, τ, needed to evaluate the effective particle diffusion parameter was calculated from the correlation [25]:

$$\tau = \frac{(2-\varepsilon_p)^2}{\varepsilon_p} \tag{24}$$

2.5. Method of calculation of numerical solutions of the models

The coupled system of the mass balance and the heat balance equations was solved using a method previously described in details in [4]. First, the steady-state distributions of the temperature and the pressure throughout the column were derived. Afterwards, the time dependent mass balance equation was solved, using the temperature and the pressure profiles previously obtained. The heat balance and the differential mass balance equations were solved using the method of orthogonal collocation on finite elements (OCFE) in its analog version previously described [35]. The spatial derivatives were discretized, following the OCFE method. The set of ordinary differential equations obtained through this process was then solved using the VODE solver [36].

3. Experimental

The experiments and their results were described in detail in earlier papers [18,19]. In the following section, we briefly describe the experimental conditions.

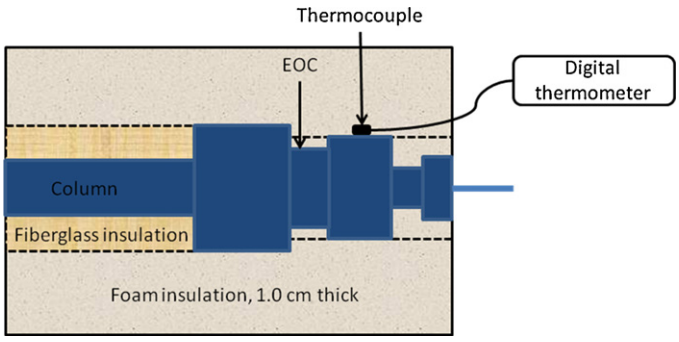

Fig. 1. Method of column insulation and detail of endfitting with thermocouple. The arrow labeled EOC marks the approximate location of the end of the column.

3.1. Apparatus

The SFC system was constructed in-house and consisted of an ISCO model 260D syringe pump, a helium-actuated Valco CI4W injector with a 60-nL internal sample loop, and a Varian model 2740 gas chromatograph with flame ionization detector. The injector was placed in the column oven and a thermal conditioning coil was placed within the oven upstream from the injector to preheat the mobile phase to the column oven temperature. Pressure transducers were connected to tees placed immediately before the injector and at the column outlet, and the column outlet pressure was adjusted with nitrogen. Additional details of the flow and pressure control are provided in earlier papers [18,37]. Data were acquired using a high-speed chromatography data acquisition system (VG Data Systems Chromatography Server, 22-bit A/D conversion rate at 960 Hz) and Thermo LabSystems XChrom software. The sampling frequency was varied from 30 to 240 Hz depending on the flow rate to provide at least 30 data points over the half-width of the narrowest peak. All peaks were analyzed using the manual integration utility included with the software.

Two columns packed with Spherisorb C8 (Waters Corporation, Milford, MA 01757, USA) were used. Particle diameters were 3 and 5 μm. The column dimensions were 2.0 mm × 150 mm with stainless steel walls and fittings. The external column wall diameter was 6.4 mm. The total porosity of 0.724 for the 5-μm column and 0.784 for 3-μm column was measured by pycnometry. We assumed an external porosity of 0.400 for the 5-μm column and 0.421 for 3-μm column, yielding ξ equal about 150 in the Blake, Kozeny, and Carman equation.

For studies on the effects of the thermal conditions, the columns were configured in one of two ways. For the thermostatted case, the steel wall of the column was exposed to the oven air in the typical fashion. The thermostat temperature was equal 50 °C. For the insulated case, the column was covered with fiberglass and foam pipe insulation and suspended in the oven as presented in Fig. 1. The column inlet and outlet temperatures were monitored with small button-style surface-probe thermocouples connected to the column endfitting and also covered with insulation. The column connections were made with short lengths 0.18 mm i.d. × 1.6 mm o.d. stainless steel tubing.

3.2. Chemicals

Carbon dioxide was SFC grade with no helium. Methane was 99 mol% pure. Both were obtained from Scott Specialty Gases, Troy, MI, USA. Solutions of methane in CO_2 were prepared by introducing up to 500 μL of the neat alkane mixture into an open 150-mL stainless steel vessel, followed by gaseous methane to a gauge pressure of 1–2 bar.

The vessel was then sealed with a pressure relief valve at one end and liquid CO_2 was introduced through a valve at the opposite end up to a pressure of 120 bar at ambient temperature.

3.3. Chromatography

Samples for injection were prepared in CO_2 as described in the preceding section. A connection was made between the valve of the pressurized sample container and the sample port of the injector with a length of 1.6-mm o.d. stainless steel tubing. Sample injection was accomplished by temporarily opening a valve connected to the waste port of the injector and allowing the pressurized sample to vent through a restrictor fabricated from a short length of 1.6-mm o.d. stainless steel tubing which was crimped on the outlet end.

The mobile phase in the syringe pump was maintained at −2.0 °C, and the detector temperature was 250 °C. The pump was operated in constant flow mode set to within 0.001 mL/min, and the outlet pressure was adjusted as described earlier. Injections for each set of conditions were done in triplicate and an equilibration time of 10–15 min was allowed after changes in the flow rate. Stable pressure readings and a constant temperature at the column outlet were taken to indicate steady-state flow and thermal conditions. When the flow rate was increased the outlet pressure was decreased (and inlet pressure increased) to maintain a constant temporal average density [18].

4. Results and discussion

To validate the heat and mass transfer models presented in theoretical section, we compare the results of the calculation to the experimental data obtained, which are the dependence on the mobile phase flow rate of the temperature, the pressure, the retention factor of the unretained tracer, and the column efficiency. In this work the flow rate was always referenced to the flow rate of the pump. To simulate the chromatography process, the flow rate at the column inlet was calculated assuming constant mass flux condition.

The validation was made for the insulated column as well as for the column kept in the air bath. The average reduced density (RD) was either RD = 1.0 or RD = 1.5. The experimental data were taken from results previously published [18,19].

4.1. Temperature and pressure distribution

To calculate the temperature and the pressure distributions for different columns, under different experimental conditions, the sets of Eqs. (1)–(6) and (16)–(19) were solved to obtain the values under steady-state conditions. The ξ parameter in the Blake, Kozeny, and Carman equation (17) was estimated as the one that gives the best agreement between the measured and the calculated outlet pressures. This value was equal to 151 for the 5-μm column, 150 for the 3-μm column working in the air bath and between 144 and 154 for the 3-μm column when it is insulated.

Two last parameters are needed for the calculations, the effective thermal conductivity and the effective heat transfer coefficient. As it was stated above, the effective thermal conductivity was evaluated from Eq. (20). The CO_2 conductivity was calculated from the results of Vesovic et al. [31]. The solid state conductivity was also calculated from Eq. (20) taking into account that the carbon load for Waters Spherisorb C8 column is 5.8%. The λ_S was evaluated to be about 1.07, assuming the conductivity of silica to be equal to 1.4 and that of the C8 ligands to be equal to 0.117 W/(m K). In the case of the air bath experiment, the effective heat transfer coefficient, h_e (see Eq. (6)) was estimated from the results of temperature measurements made at the column end, at the highest flow rate (which gives the highest temperature drop). The values obtained

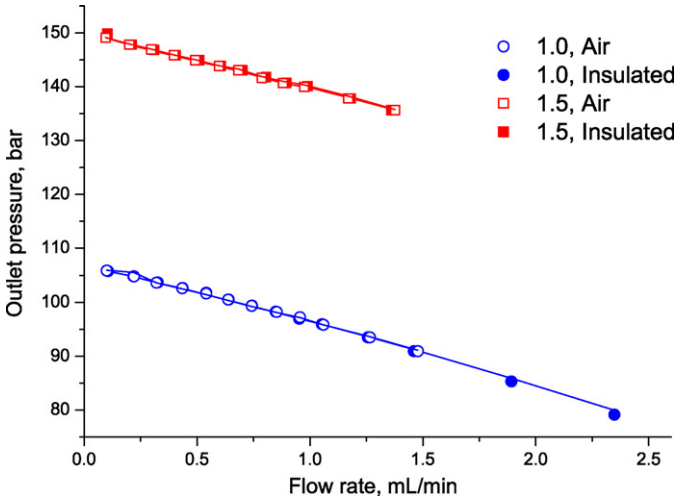

Fig. 2. Outlet pressure vs. flow rate for the column packed with 5 μm particles. The flow rates are those of the liquid mobile phase at the pump. Symbols: experimental results, solid lines: calculated results.

were 120 $W/m^2/K$ for the 5-μm column and 75 $W/m^2/K$ for the 3-μm column, respectively. The same values were used at the other flow rates. In the case of the insulated column, the heat transfer coefficient was assumed to be zero.

The calculated and measured, outlet pressures are compared in Figs. 2 and 3 for both columns. The agreement achieved is very good, the difference between the calculated and the measured pressures was always less than 1%.

Figs. 4 and 5 compare the calculated temperatures of the column wall, at the column outlet and the measured temperature of the outlet endfitting, for both columns. The agreement achieved is very good for data obtained under air bath conditions. However, for the insulated column, the calculated temperature was always lower than the one measured, especially for the column packed with 3 μm particles, in which case the calculated and experimental temperatures differ by about 4 °C. There are at least three possible reasons for this disagreement: (1) the thermal insulation of the column might not be perfect; (2) heat conducted from the connecting tubing and the small nut at the end, which were exposed to the surrounding air, might have raised the temperature of the endfitting (see Fig. 1); and (3) heat might have been conducted along the column steel wall. The very high thermal conductivity of steel causes

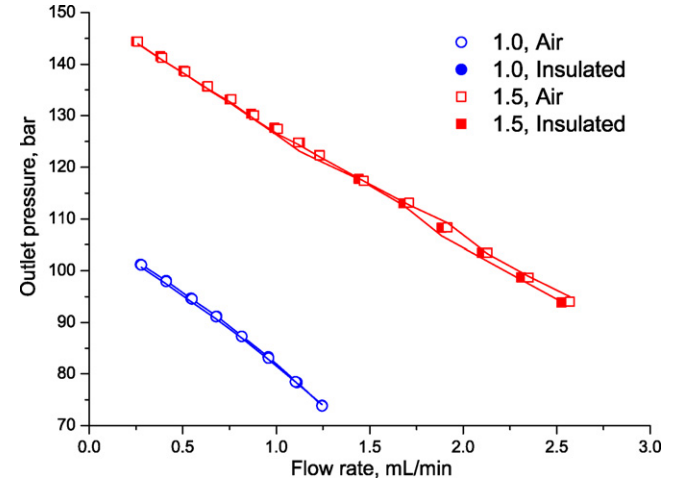

Fig. 3. Outlet pressure vs. flow rate for the column packed with 3 μm particles. The flow rates are those of the liquid mobile phase at the pump. Symbols: experimental results, solid lines: calculated results.

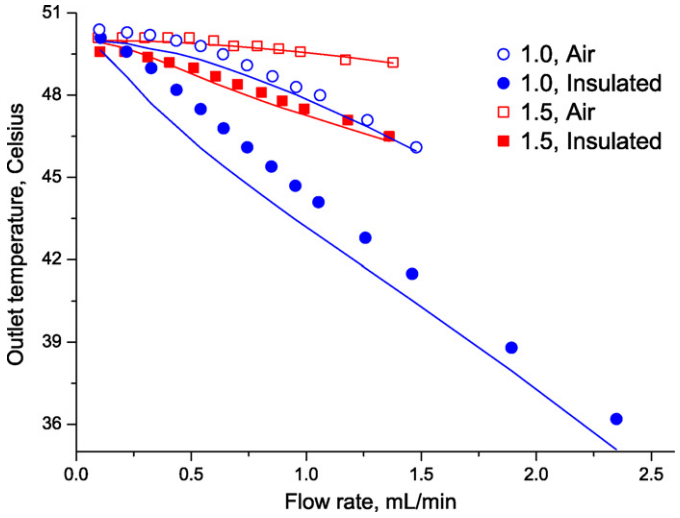

Fig. 4. Outlet temperature vs. the flow rate for the column packed with 5 μm particles. Temperatures measured at the surface of the endfittings. The flow rates are those of the mobile phase at the pump. Symbols: experiment data, solid lines: calculation results.

the temperature to stabilize along the wall—see Fig. 10. The extent of this stabilization depends on the wall thickness. The thicker is the wall, the higher the heat flux and the flatter the temperature distribution. In our calculations we did not take into account the influence on the wall temperature distribution of the heat conduction by the massive endfittings. If the endfittings were taken into account, the calculated temperature would be higher than if they are ignored. However, it is difficult to include them into the calculations because of their complicated shapes. Taking these points into account, it seems that the actual fluid temperature near the column wall, at the outlet of the insulated column should be between the calculated and the measured values.

4.2. Retention time of the unsorbed solute and column efficiency

To validate the mass balance model, expressed by Eqs. (7)–(14) and (21)–(24), we compared the calculated and measured retention times and the calculated and measured column efficiencies. These comparisons were performed for methane, which can be regarded

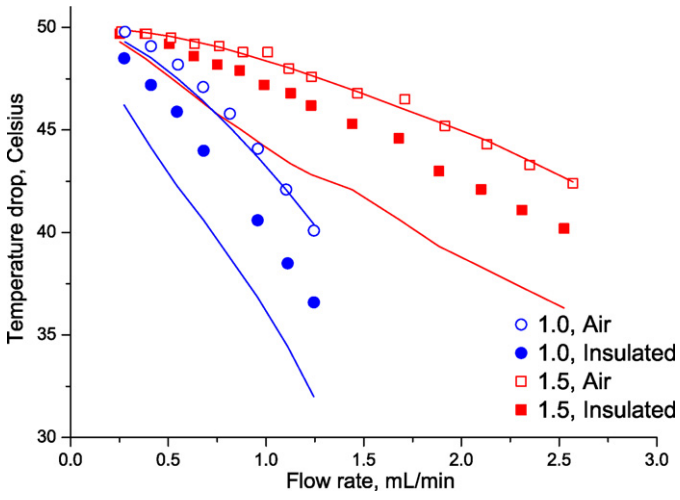

Fig. 5. Outlet temperature vs. the flow rate for the column packed with 3 μm particles. Temperatures measured at the surface of the endfittings. The flow rates are those of the mobile phase at the pump. Symbols: experiment data, solid lines: calculation results.

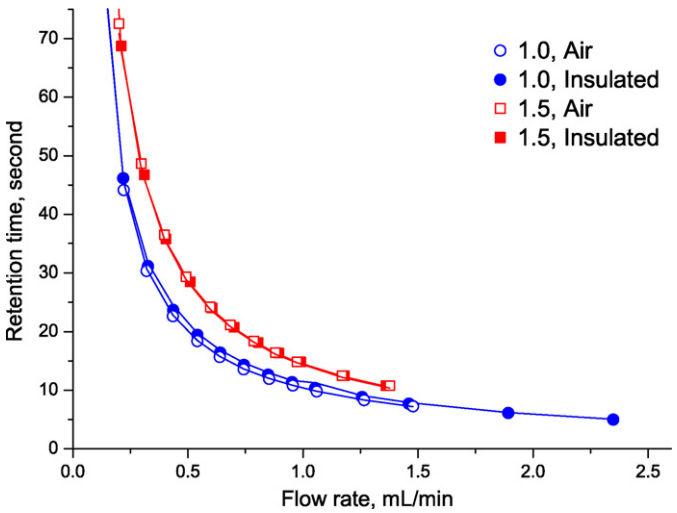

Fig. 6. Retention time vs. flow rate for the column packed with 5 μm particles. The flow rates are for the mobile phase at the pump. Symbols: experimental data, solid lines: calculated results.

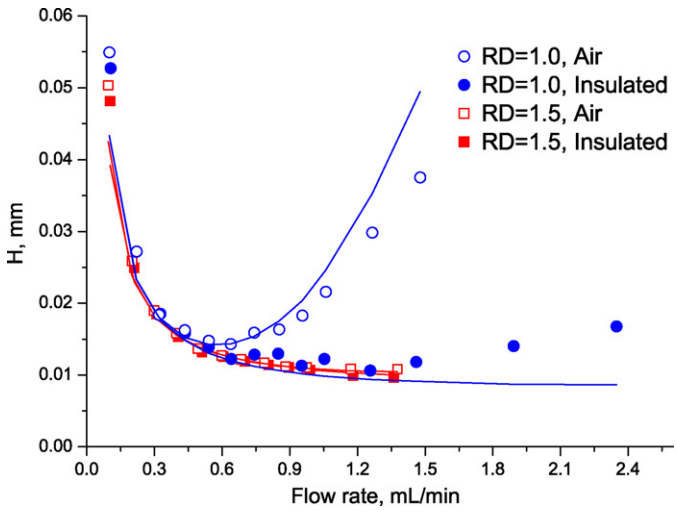

Fig. 8. HETP vs. the flow rate for the column packed with 5 μm particles. The flow rates are for those measured at the pump. Symbols: experimental data, solid lines: calculated results.

as unretained [18]. Before performing the systematic calculations, the parameter γ_2 in Eq. (22) must be estimated on the basis of the experimental data. We chose the value of γ_2 that provides the best agreement between the experimental and the theoretical peak profiles. The calculations were performed for both columns and all the sets of experimental conditions (air bath, insulated column, RD = 1.0 and RD = 1.5) but for only one mobile phase flow rate. We chose arbitrarily a flow rate of about 0.6 mL/min, which is a flow rate at which the column efficiency is close to its maximum value. In the case of the column packed with 5 μm particles, the values obtained for γ_2 were equal to 1.42 for RD = 1.0 and 1.7 for RD = 1.5. However, in the case of the column packed with 3 μm particles, the values obtained for γ_2 were equal to 0.6 for RD = 1.0 and the column in the air bath and $\gamma_2 = 4$ and the insulated column. In the case of RD = 1.5 the value of γ_2 was equal to 3.5.

The calculated and the measured retention times of methane are compared in Figs. 6 and 7. The agreement between calculated and experimental results is excellent for both columns.

The comparison between the calculated and the measured HETP for methane is presented in Figs. 8 and 9 for both columns. The agreement in all cases, except for RD = 1.0 and the insulated column, is good. The disagreement in this last case is probably due to an insufficient thermal insulation.

4.3. Distributions of physico-chemical parameters inside the columns

In SFC, the distributions of the temperature, the density, the viscosity and the flow velocity of the mobile phase strongly depend on the pressure difference between column inlet and outlet and on the average reduced density and the working conditions of the column (column in an air bath or insulated column).

To estimate how large are the gradients of these parameters we show in Figs. 10–14 the results of calculations made for RD = 1, with the column packed with 3 μm particles, working in air at a flow rate of 1.245 mL/min. As can be seen, the temperature difference between the column inlet and outlet is 20 K while the difference between the temperatures in the column center and at the wall may reach almost 8 K over a distance of only 1 mm. Still more dramatic are the changes in the mobile phase density. The CO_2 density at the column outlet, near the column wall, can be three times smaller

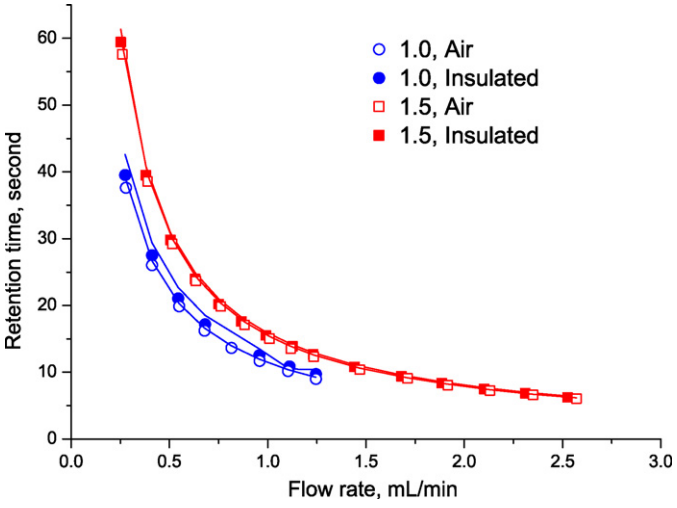

Fig. 7. Retention time vs. flow rate for the column packed with 3 μm particles. The flow rates are for the mobile phase at the pump. Symbols: experimental data, solid lines: calculated results.

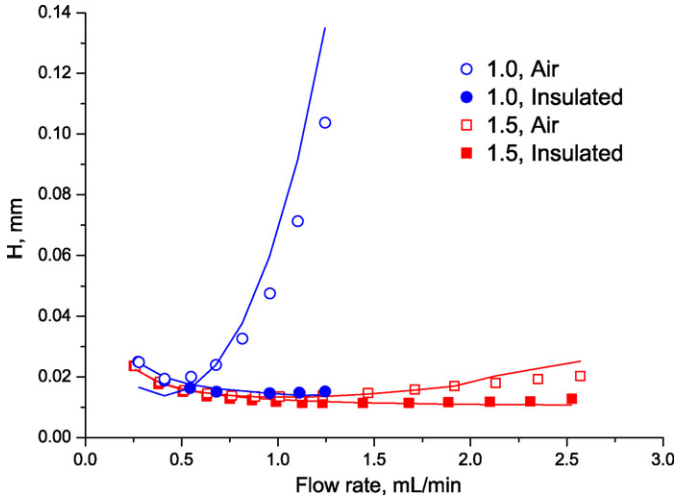

Fig. 9. HETP vs. the flow rate for the column packed with 3 μm particles. The flow rates are for those measured at the pump. Symbols: experimental data, solid lines: calculated results.

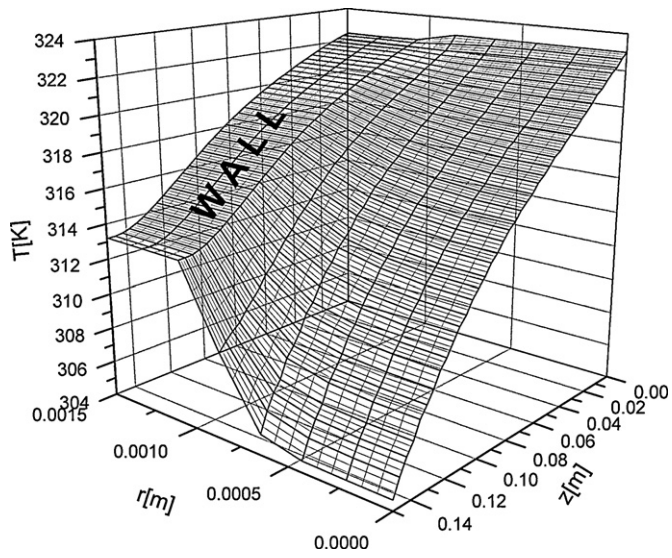

Fig. 10. Calculated temperature distribution for the column packed with 3 μm particles, at a flow rate of 1.245 mL/min.

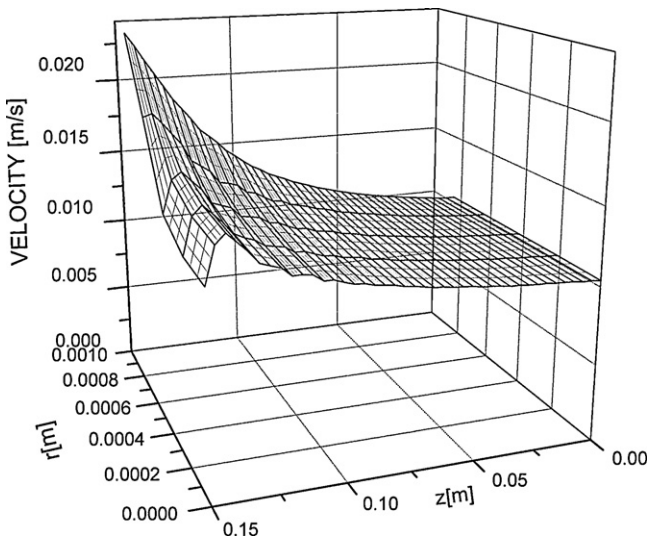

Fig. 13. Velocity distribution for the 3 μm column at a flow rate of 1.245 mL/min.

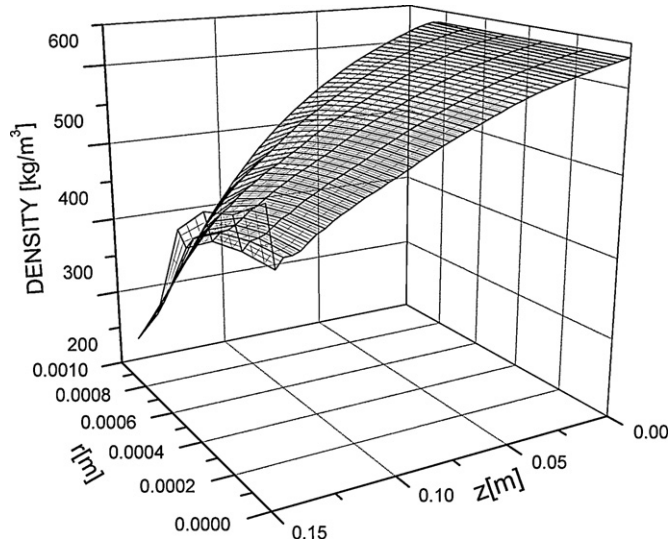

Fig. 11. Density distribution for the 3 μm column at a flow rate of 1.245 mL/min.

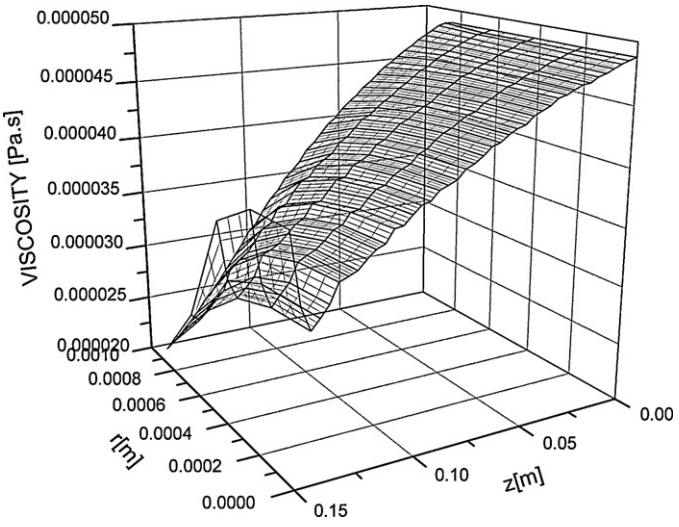

Fig. 12. Viscosity distribution for the 3 μm column at a flow rate of 1.245 mL/min.

than it is at the column inlet. The ratio of the mobile phase density in the column center and close to the column wall can reach 2.5. Similar changes are observed for the mobile phase viscosity. It should be noticed that, near the end of the column, the fluid conditions are close to the critical conditions, which is why the density and the viscosity of CO_2 vary so rapidly.

The large density and viscosity decrease along the column and in the radial direction, from the center to the column wall cause important increases of the axial velocity, by more than two times, and in the radial direction, by close to two times. The radial component of the velocity, calculated from Eq. (19), is more than 1000 times smaller than its axial component, which is why it can be ignored in the calculations of the mass transfer.

The patterns of the distributions of the physico-chemical parameters previously discussed are the same at lower flow velocities and for higher average values of the reduced density, however the gradients of these parameters decrease rapidly with decreasing flow rate and increasing reduced density. This explains why the column efficiency appears to be higher for a reduced density equal to 1.5 and at high flow rates.

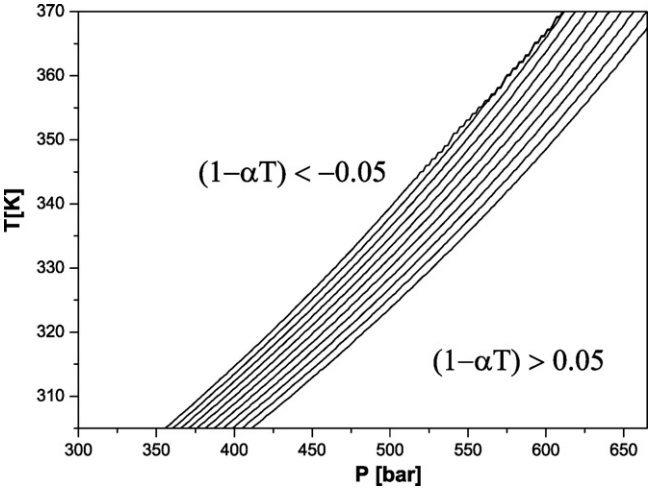

Fig. 14. Area of experimental conditions in which the parameter $(1 - \alpha T)$ is in the interval $(-0.05, +0.05)$ and the temperature gradients are negligible.

4.4. Under which experimental conditions could the radial temperature gradient be made flat everywhere?

The column efficiency would reach the maximum possible value if the radial gradients of the physico-chemical parameters would disappear. The radial gradients of the density, the viscosity and the velocity are all due to the radial temperature gradient, which is caused by heat flowing from the column wall inside the bed to compensate the heat absorbed by the mobile phase expansion. The radial and axial temperature gradients would disappear if the heat generated by viscous friction would be exactly compensated by the heat absorbed by the expansion of the mobile phase. This takes place when the term $(1 - \alpha T)$ in Eq. (1) becomes close to zero.

The conditions under which this term is close to zero are illustrated in Fig. 14. Numerical calculations performed under the conditions indicated by the area labeled in Fig. 14 confirm that the changes in temperature along and across the column are then negligible (figure not presented). Experimental measurements are in progress to verify this prediction. The results will be presented later.

5. Conclusions

A general SFC model coupling the heat and the mass balance equations is proposed. Numerical solutions of the heat balance are in good agreement with the temperature measured at the outlet endfitting of the column and with the pressure drop measured along the column. The calculation of the temperature distribution requires the prior estimate of the external heat transfer coefficient. This coefficient can be estimated on the basis of the column wall temperature measured at the highest mobile phase flow.

The numerical solution of the generalized ED model coupled with the calculated temperature and pressure distributions enables excellent forecasts of the retention times and efficiency for elution of an unsorbed solute. Implementation of the mass balance model required estimates of the parameters, most of which are provided by simple experiments or by commonly accepted correlations but one has to be derived from a single experiment performed at a moderate flow rate, close to the optimum flow rate for minimum plate height.

The model of coupled heat and mass transfer that we proposed in this work needs now to be validated for retained compounds. The influence of the temperature, the pressure, and the density of the mobile phase on the equilibrium constants of such compounds will have to be estimated and/or measured to permit the calculation of their elution peak profiles. Work is currently in progress on this topic. Obviously, as in HPLC, this model could be extended to preparative applications, in which the equilibrium isotherms of the compounds studied in the column system are no longer linear.

Finally, our work suggests that the performance of SFC at high velocities, using long columns packed with fine particles, could possibly exceed most current expectations. This would be achieved if practical applications could be developed using SFC in the range of experimental conditions in which the two heat effects, the one due to viscous friction and the one due to the mobile phase expansion, would cancel each other.

Nomenclature

C	concentration in mobile phase
c_p^m	mobile phase heat capacity
c_s	solid phase heat capacity
c_w	wall heat capacity
d_p	adsorbent diameter
D_{eff}	effective particle diffusivity
$D_{z,a}$	axial apparent dispersion coefficient
D_L	axial dispersion coefficients
$D_{r,a}$	radial apparent dispersion coefficient
D_m	molecular diffusion coefficient
F	phase ratio
h_e	effective heat transfer
k_{ext}	external mass transfer coefficient
L	column length
N	number of theoretical plates
q	concentration in stationary phase
P	pressure
R_i	internal column wall radius
R_e	external column wall radius
R_p	the particle radius
RD	reduced density
t	time
t_p	injection time
T	temperature
u	superficial velocity
V_m	partial molar volume
w	interstitial velocity

Greek symbol

α	coefficient of thermal expansion
ε_e	external porosity
ε_t	total column porosity
ε_p	particle porosity
γ_1, γ_2	geometrical constant
η	viscosity
$\lambda_{r,ef}$	effective bed conductivity
λ_w	wall heat conductivity density
τ	tortousity parameter
ξ	empirical parameter in Eq. (17)

Subscripts

ext	external
F,0	inlet value
r	radial direction
z	axial direction

Acknowledgment

This work was partially supported by grant N N204 002036 of the Polish Ministry of Science and Higher Education.

References

[1] G. Terfloth, J. Chromatogr. A 906 (2001) 301.
[2] F. Denet, W. Hauck, R.M. Nicoud, O. Di Giovanni, M. Mazzotti, J.N. Jaubert, M. Morbidelli, Ind. Eng. Chem. Res. 40 (2001) 4603.
[3] S. Peper, M. Lubbert, M. Johannsen, G. Brunner, Sep. Sci. Technol. 37 (2002) 2545.
[4] K. Kaczmarski, J. Kostka, W. Zapała, G. Guiochon, J. Chromatogr. A 1216 (2009) 6560.
[5] J. Kostka, F. Gritti, G. Guiochon, K. Kaczmarski, J. Chromatogr. A 1217 (2010) 4704.
[6] H.G. Janssen, H.M.J. Snijders, J.A. Rijks, C.A. Cramers, P.J. Schoenmakers, J. High Resolut. Chromatogr. 14 (1991) 438.
[7] X. Lou, H.G. Janssen, H. Snijders, C.A. Cramers, J. High Resolut. Chromatogr. 19 (1996) 449.
[8] A. Rajendran, O. Kraeuchi, M. Mazzotti, M. Morbidelli, J. Chromatogr. A 1092 (2005) 149.
[9] A. Rajendran, T.S. Gilkison, M. Mazzotti, J. Sep. Sci. 31 (2008) 1279.
[10] P.J. Schoenmakers, HRC & CC, J. High Resolut. Chromatogr. Chromatogr. Commun. 11 (1988) 278.
[11] P.A. Mourier, M.H. Caude, R.H. Rosset, Chromatographia 23 (1987) 21.
[12] C. Bouigeon, D. Thiebaut, M. Caude, Anal. Chem. (Washington, DC, United States) 68 (1996) 3622.
[13] D.R. Gere, R. Board, D. McManigill, Anal. Chem. (Washington, DC, United States) 54 (1982) 736.
[14] T.A. Berger, J.F. Deye, Chromatographia 31 (1991) 529.

[15] T.A. Berger, W.H. Wilson, Anal. Chem. (Washington, DC, United States) 65 (1993) 1451.
[16] U. Koehler, P. Biermanns, E. Klesper, J. Chromatogr. Sci. 32 (1994) 461.
[17] U. Koehler, E. Klesper, J. Chromatogr. Sci. 32 (1994) 525.
[18] W. Xu, D.L. Peterson, J.J. Schroden, D.P. Poe, J. Chromatogr. A 1078 (2005) 162.
[19] D.P. Poe, J.J. Schroden, J. Chromatogr. A 1216 (2009) 7915–7926.
[20] I. Halasz, R. Endele, J. Asshauer, J. Chromatogr. 112 (1975) 37.
[21] H. Poppe, J.C. Kraak, J.F. Huber, Chromatographia 14 (1981) 515.
[22] H.-J. Lin, C. Horvath, Chem. Eng. Sci. 56 (1981) 47.
[23] H. Poppe, J.C. Kraak, J. Chromatogr. 282 (1983) 399.
[24] D. Antos, K. Kaczmarski, W. Piatkowski, A. Seidel-Morgenstern, J. Chromatogr. A 1006 (2003) 61.
[25] G. Guiochon, A. Felinger, A.M. Katti, D. Shirazi, Fundamentals of Preparative and Nonlinear Chromatography, second ed., Elsevier, Amsterdam, 2006.
[26] D. Horne, J.H. Knox, L. McLaren, Sep. Sci. 1 (1966) 531.
[27] J.H. Knox, G.R. Laird, P.A. Raven, J. Chromatogr. 122 (1976) 129.
[28] R.B. Bird, W.E. Stewart, E.N. Lightfoot, Transport Phenomena, John Wiley & Sons, 2002.
[29] R. Span, W. Wagner, J. Phys. Chem. Ref. Data 25 (1996) 1509.
[30] A. Fenghour, W.A. Wakeham, V. Vesovic, J. Phys. Chem. Ref. Data 27 (1998) 1.
[31] V. Vesovic, W.A. Wakeham, G.A. Olchowy, J.V. Sengers, J.T.R. Watson, J. Millat, J. Phys. Chem. Ref. Data 19 (1990) 763.
[32] Y.P. Zarichnyak, V.V. Novikov, Inzhenerno-Fizicheskii Zhurnal 34 (1978) 648.
[33] E.J. Wilson, C.J. Geankoplis, Ind. Eng. Chem. Fundam. 5 (1966) 9.
[34] P.R. Sassiat, P. Mourier, M.H. Caude, R.H. Rosset, Anal. Chem. (Washington, DC, United States) 59 (1987) 1164.
[35] K. Kaczmarski, G. Storti, M. Mazzotti, M. Morbidelli, Comput. Chem. Eng. 21 (1997) 641.
[36] P.N. Brown, A.C. Hindmarsh, G.D. Byrne, available at http://www.netlib.org.
[37] D.P. Poe, P.J. Marquis, T. Tomlinson, J. Dohm, J. He, J. Chromatogr. A 785 (1997) 135.